

Accepted Manuscript

Synthesis, crystal growth, thermal, electronic and vibrational spectral studies of 1-(4-Bromophenyl)-3-(3, 4-dimethoxy-phenyl) prop-2-en-1-one: A density functional theory study

L. Joseph, B.S. Arunsasi, D. Sajan, V. Shettigar

PII: S0022-2860(14)00827-8

DOI: <http://dx.doi.org/10.1016/j.molstruc.2014.08.008>

Reference: MOLSTR 20868

To appear in: *Journal of Molecular Structure*

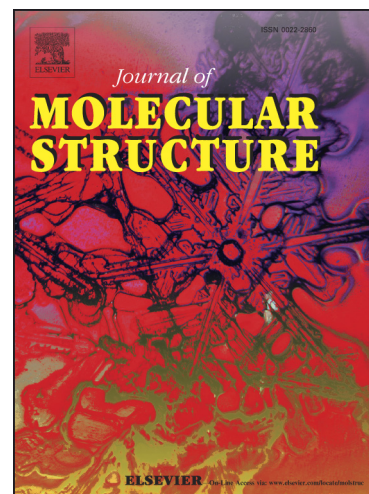
Received Date: 6 June 2014

Revised Date: 2 August 2014

Accepted Date: 2 August 2014

Please cite this article as: L. Joseph, B.S. Arunsasi, D. Sajan, V. Shettigar, Synthesis, crystal growth, thermal, electronic and vibrational spectral studies of 1-(4-Bromophenyl)-3-(3, 4-dimethoxy-phenyl) prop-2-en-1-one: A density functional theory study, *Journal of Molecular Structure* (2014), doi: <http://dx.doi.org/10.1016/j.molstruc.2014.08.008>

This is a PDF file of an unedited manuscript that has been accepted for publication. As a service to our customers we are providing this early version of the manuscript. The manuscript will undergo copyediting, typesetting, and review of the resulting proof before it is published in its final form. Please note that during the production process errors may be discovered which could affect the content, and all legal disclaimers that apply to the journal pertain.



Synthesis, crystal growth, thermal, electronic and vibrational spectral studies of 1-(4-Bromophenyl)-3-(3, 4-dimethoxy-phenyl) prop-2-en-1-one: A density functional theory study

L Joseph^{1,4}, B S Arunsasi^{1,2}, D Sajan^{1*} and V Shettigar³

¹Department of Physics, Bishop Moore College, Mavelikara, Alappuzha -690110, Kerala, India

²Department of Physics and Research Centre, Scott Christian College (Autonomous), Nagercoil-629003, Tamil Nadu, India

³Department of Physics, Gokhale Centenary College, N.H.17, Vandige, Ankola-581314, India.

⁴Department of Physics, C M S College, Kottayam -686001, Kerala, India

E-mail: dsajand@gmail.com , dsajanbmc@gmail.com (D. Sajan)

Abstract. A new chalcone derivative, 1-(4-Bromophenyl)-3-(3,4-dimethoxy-phenyl)prop-2-en-1-one (DMBC) was synthesized and single crystals were grown by slow evaporation technique. The FT-Raman and FT-IR spectra of the sample were recorded in the region 3500-50 cm⁻¹ and 4000-400 cm⁻¹ respectively. The spectra were interpreted with the aid of normal coordinate analysis, following structure optimizations and force field calculations based on density functional theory (DFT) at the B3LYP/6-31G(d,p) level of theory. Normal coordinate calculations were performed using the DFT force field corrected by a recommended set of scaling factors yielding fairly good agreement between the observed and calculated wavenumbers. DMBC is thermally stable up to 265.0 °C and optically transparent in the visible region. The total electron density and Molecular electrostatic potential surfaces of the molecules were constructed by Natural Bond Orbital analysis using B3LYP/6-311++G(d,p) method to display electrostatic potential (electron + nuclei) distribution, molecular shape, size, and dipole moments of the molecule. The electronic properties, HOMO and LUMO energies were measured.

1. Introduction

Organic molecules, especially chalcone derivatives, constitute an important group of natural products and some of them possess a wide range of biological activities such as antimicrobial, anticancer, antiviral etc [1-4]. Chalcones have the common skeleton of 1, 3-diaryl-2-propen-1-one and belong to the flavonoid family. Moreover chalcones belong to nature products and have low toxicity. Some derivatives

* Corresponding author. Tel.: +919495043765; Fax: +914792303230;

E-mail address: dsajand@gmail.com , dsajanbmc@gmail.com (D. Sajan).

are used as sweeteners, drugs, and sunscreen agents. Chalcone and its derivatives are very versatile as physiologically active compounds and substrates for the evaluation of various organic syntheses [5-8]. They also serve as a back bone for the synthesis of various heterocyclic compounds. Furthermore, many chalcone derivatives are a class of organic compounds with excellent NLO properties [9-12], much better than those observed in inorganic crystals. They have recently received considerable attention owing to their potential application in photonic device applications such as erasable memory media and optical switching. Recently, it has been noted that, among many organic compounds reported for their second harmonic generation, chalcone derivatives are known for their excellent blue light transmittance and good crystallizability [10-12]. Owing to their good thermal stability, associated with high laser damage resistance and transparency, this family of compounds has been used in recent years for frequency doubling of diode lasers down to 470 nm [13]. The addition of various substituents to the chalcone molecules allows us to control their NLO properties.

The structural studies on the chalcone derivative, 1-(4-Bromophenyl)-3(3, 4-dimethoxy-phenyl) prop-2-en-1-one (DMBC) have been reported earlier [14]. However, to the best of our knowledge no detailed studies on DMBC have been made so far. Recently density functional theory (DFT) has emerged as a powerful tool for analysing vibrational spectra of fairly large molecules. The application of DFT to chemical systems has received much attention because of faster convergence in time than traditional quantum mechanical correlation methods [15-23]. In this paper, we report for the first time, the bulk growth, structural, electronic, thermal and detailed vibrational spectral investigation of DMBC using the scaled quantum mechanical (SQM) force field technique [24] based on density functional theory (DFT) calculations.

2. Experimental

2.1 Synthesis of the compound

The chalcone derivative was synthesized by the Claisen–Schmidt condensation reaction [25]. The title compound was obtained by the condensation of 3, 4 dimethoxy benzaldehyde (0.01 mol) with 4-

bromoacetophenone (0.01 mol) in ethanol (60mL) in the presence of NaOH (5mL, 20%). After stirring, the content of the flask was poured into ice-cold water (20mL) and the resulting crude solid was collected by filtration. The compound was dried and purified by repeated recrystallization from acetone. The molecular structure of the chalcone derivative under study is shown in figure 1.

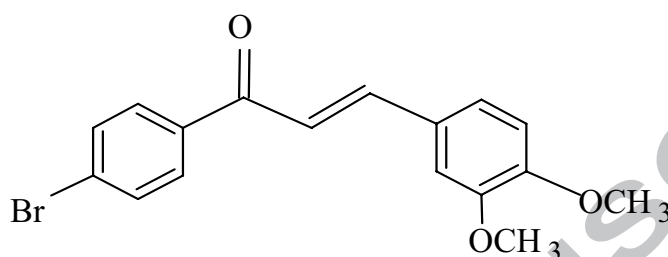


Figure 1. Molecular structure of the synthesized compound of DMBC

2.2 Crystal growth

Single crystals of DMBC were grown by the slow evaporation solution growth technique from the acetone solution at room temperature. Pale yellowish, high-quality DMBC single crystals with a maximum dimension of $12 \times 5 \times 1.3 \text{ mm}^3$ were grown in a period of 10 days. DMBC crystallizes in space group $P2_1/c$ with eight molecules ($Z=8$) in the unit cell with a volume of $2930.17 (10) \text{ \AA}^3$. From the single crystal XRD data [25] it is observed that the crystal belongs to monoclinic system with the following cell dimensions: $a=31.3937 (5) \text{ \AA}$, $b=4.0139 (1) \text{ \AA}$, $c=25.2400 (4) \text{ \AA}$, $\beta=112.885^\circ$. The grown crystals are shown in figure 2



Figure 2. Photograph of the crystal DMBC.

2.3 FT-IR, FT-Raman, UV-Vis Spectra and Thermal Studies

The FT-IR spectrum was recorded by KBr pellet technique using Thermo Nicolet AVATAR 370 DTS FT-IR spectrometer working in the wave number range 4000-400 cm^{-1} . The data were collected at 4 cm^{-1} resolution. The FT-Raman spectrum of the sample was recorded between the 3500-50 cm^{-1} regions on a RFS 100/s FT-Raman spectrophotometer. With an Nd:YAG laser at 1064 nm and output of 300 mW used as the excitation source and with a liquid nitrogen cooled Ge-didode detector, 1000 scans accumulated for over 30 min duration. The resolution after apodization was 2 cm^{-1} . The UV-Vis absorption spectrum of the sample was recorded in acetone solution using a Shimadzu UV-Vis spectrophotometer in the spectral region of 200-400 nm. Thermogravimetric analysis (TGA) was carried out to investigate the thermal stability [26] under nitrogen atmosphere at a heating rate of 10/min using the Perkin Elmer simultaneous TGA/DTA analyzer.

3. Quantum chemical calculation

The quantum chemical calculation has been performed using the B3LYP level of theory supplemented with the standard 6-31G (d,p) basis set, using the Gaussian '09 program [27] to calculate optimized bond lengths, bond angles, atomic charges, and vibrational wavenumbers with their IR intensities and Raman scattering activities. After the most stable conformer of the title compound was determined, geometry optimizations of this conformer have been performed with the 6-31G (d,p) basis set and the hybrid B3LYP functional approach. The cartesian representation of the theoretical force constants has been computed at the fully optimized geometry by assuming $P2_1/c$ point group symmetry. Scaling of the force fields were performed by the scaled quantum mechanical (SQM) procedure

$$F_{ij}^{scaled} = \sqrt{C_i C_j} F_{ij}^{B3LYP} \quad (1)$$

where C_i is the scale factor of coordinate i , F_{ij}^{B3LYP} is the B3LYP/6-31G(d,p) force constant in the local internal coordinates, and F_{ij}^{scaled} is the scaled force constant. The multiple scaling of the force constants was performed by the quantum chemical method with selective scaling in the local symmetry coordinate representation [28, 29], using transferable scale factors available in the literature [19]. Selective scaling

was done using a set of 11 transferable scale factors giving an RMS wavenumber 9.46 cm^{-1} . The transformation of the force field from cartesian to symmetry coordinate, the scaling, the subsequent normal coordinate analysis and calculations of total energy distribution (TED), IR and Raman intensities, were done on a PC with the version V7.0-G77 of the MOLVIB programme written by Sundius[30, 31].

The Raman activities (S_i) calculated by Gaussian 09 program were converted to relative Raman intensities (I_i), using the following relationship from the basic theory of Raman scattering [32, 33]

$$I_i = \frac{f(\nu_o - \nu_i)^4 S_i}{\nu_i \left[1 - \exp\left(\frac{-hc\nu_i}{kT}\right) \right]} \quad (2)$$

where ν_o is the exciting frequency (in cm^{-1} units), ν_i is the vibrational wavenumber of the i^{th} normal mode, h , c and k are universal constants, and f is a suitably chosen common scaling factor for all the peak intensities. Raman and infrared spectra were simulated using a pure Lorentzian band profile (fwhm= 10cm^{-1}).

4. Result and discussion

4.1 NMR spectra

The Nuclear Magnetic Resonance (NMR) spectrum was recorded to confirm the presence of various types of protons for the formation of the target compound. The recorded NMR spectrum is shown in figure 3. The aromatic protons of the bromophenyl moiety appear as two doublets at $\delta=8.1$ and 7.9 ppm, while the aromatic protons of 3-4 dimethoxyphenyl appeared as two doublets at $\delta=7.0$ and 7.3 ppm. Two closely spaced doublets at $\delta=3.7$ and 3.9 ppm correspond to the two $-\text{OCH}_3$ groups. These peaks confirm the formation of the compound.

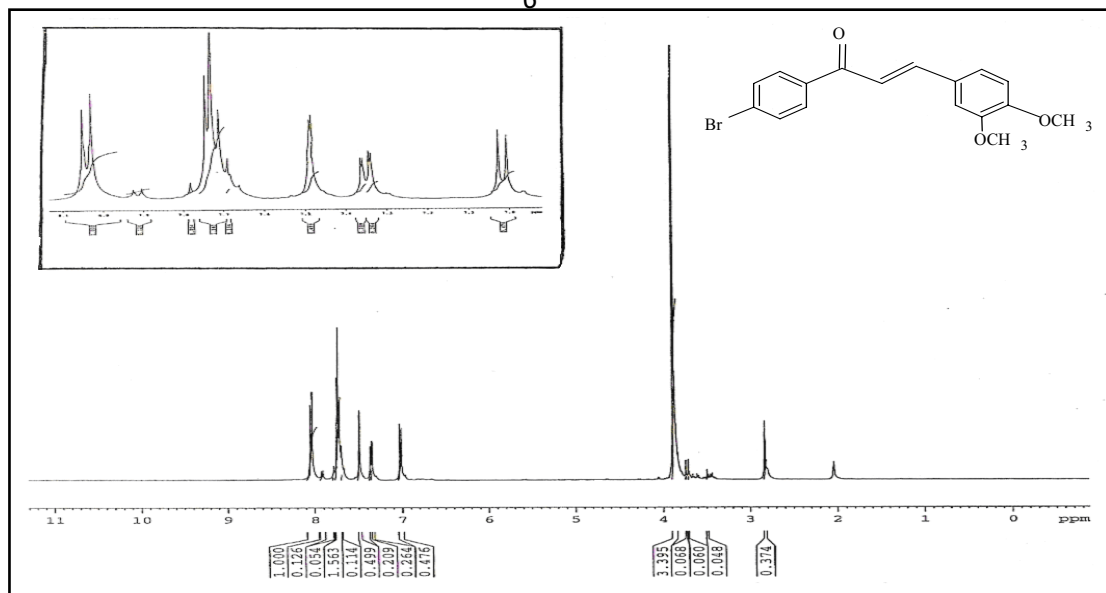


Figure 3. NMR spectrum of DMBC.

4.2 Molecular structure

The optimized structural parameters of DMBC calculated using B3LYP/6-31G(d,p) basis set are listed in table 1 along with the experimental data [14], in accordance with the atom numbering scheme in figure 4. The agreement between the experimental and optimized crystal structure is quite good showing that the geometry optimization almost exactly reproduces the experimental conformation. The molecule consists of two phenyl rings (Ph1 and Ph2) which are planar, with dihedral angles $C_5-C_4-C_3-C_{20} = 179.94^\circ$ and $C_{30}-C_{31}-C_{26}-C_{24} = 179.63^\circ$. The methoxy groups (Me1 and Me2) on the phenyl ring are coplanar, with dihedral angles $C_{16}-O_{15}-C_6-C_5 = 0.03^\circ$ and $C_8-O_7-C_1-C_2 = 0.0^\circ$. With the substitution of the electron donating methoxy groups on the benzene ring, the symmetry of the ring is distorted, yielding ring angles smaller than 120.0° at the substitution and slightly larger than 120.0° at the ortho and meta positions. Geometrical changes are observed in the aryl-O bonds, C_1-O_7 (for Me1) and C_6-O_{15} (for Me2), due to π -conjugation. The shortening of angles $C_1-O_7-C_8$ and $C_6-O_{15}-C_{16}$ is the consequence of the sharing of lone pair electrons of the methyl group with the p electrons in the ring and the interaction of these lone pair electrons with the nearby π system.

Table 1. Optimized geometric parameters of DMBC at the B3LYP/6-31G(d,p) level of theory.

Bond Lengths (Å)			Bond Angles (°)			Dihedral Angles (°)		
Parameter	6-31G(d,p)	X-Ray ^[14]	Parameter	6-31G(d,p)	X-Ray ^[14]	Parameter	6-31G(d,p)	X-Ray ^[14]
C ₁ -C ₂	1.385	1.377	C ₁ -C ₂ -C ₃	121.2	120.7	C ₁ -C ₂ -C ₃ -C ₄	-0.08	-0.05
C ₂ -C ₃	1.415	1.409	C ₂ -C ₃ -C ₄	118.2	118.5	C ₂ -C ₃ -C ₄ -C ₅	0.16	-0.4
C ₃ -C ₄	1.399	1.387	C ₃ -C ₄ -C ₅	121.2	121.7	C ₃ -C ₄ -C ₅ -C ₆	-0.11	1.4
C ₄ -C ₅	1.396	1.402	C ₄ -C ₅ -C ₆	120.3	119.1	C ₃ -C ₂ -C ₁ -O ₇	179.8	178.9
C ₅ -C ₆	1.393	1.389	C ₂ -C ₁ -O ₇	125.2	125.4	C ₂ -C ₁ -O ₇ -C ₈	-0.4	-0.0
C ₁ -O ₇	1.360	1.367	C ₁ -O ₇ -C ₈	118.0	116.3	C ₁ -O ₇ -C ₈ -H ₉	-179.5	176.8
O ₇ -C ₈	1.418	1.427	O ₇ -C ₈ -H ₉	105.9	109.4	C ₁ -O ₇ -C ₈ -H ₁₀	-60.7	-63.1
C ₈ -H ₉	1.090	0.960	O ₇ -C ₈ -H ₁₀	111.6	109.4	C ₁ -O ₇ -C ₈ -H ₁₁	61.6	56.8
C ₈ -H ₁₀	1.097	0.960	O ₇ -C ₈ -H ₁₁	111.6	109.4	O ₇ -C ₁ -C ₂ -H ₁₂	0.0	0.9
C ₈ -H ₁₁	1.097	0.960	C ₁ -C ₂ -H ₁₂	119.4	119.6	C ₂ -C ₃ -C ₄ -H ₁₃	-179.8	179.5
C ₂ -H ₁₂	1.082	0.930	C ₃ -C ₄ -H ₁₃	119.4	119.2	C ₃ -C ₄ -C ₅ -H ₁₄	179.9	178.5
C ₄ -H ₁₃	1.085	0.930	C ₄ -C ₅ -H ₁₄	119.4	120.3	C ₄ -C ₅ -C ₆ -O ₁₅	-179.9	179.0
C ₅ -H ₁₄	1.083	0.930	C ₅ -C ₆ -O ₁₅	125.2	125.0	C ₅ -C ₆ -O ₁₅ -C ₁₆	0.03	-4.0
C ₆ -O ₁₅	1.355	1.361	C ₆ -O ₁₅ -C ₁₆	118.1	117.3	C ₆ -O ₁₅ -C ₁₆ -H ₁₇	-179.9	178.5
O ₁₅ -C ₁₆	1.420	1.436	O ₁₅ -C ₁₆ -H ₁₇	105.8	109.5	C ₆ -O ₁₅ -C ₁₆ -H ₁₈	-61.1	-58.5
C ₁₆ -H ₁₇	1.090	0.960	O ₁₅ -C ₁₆ -H ₁₈	111.5	109.4	C ₆ -O ₁₅ -C ₁₆ -H ₁₉	61.2	61.4
C ₁₆ -H ₁₈	1.097	0.960	O ₁₅ -C ₁₆ -H ₁₉	111.5	109.4	C ₁ -C ₂ -C ₃ -C ₂₀	-179.9	-178.7
C ₁₆ -H ₁₉	1.097	0.960	C ₂ -C ₃ -C ₂₀	123.0	122.3	C ₂ -C ₃ -C ₂₀ -H ₂₁	178.2	-173.1
C ₃ -C ₂₀	1.454	1.461	C ₂ -C ₃ -H ₂₁	115.8	116.6	C ₂ -C ₃ -C ₂₀ -C ₂₂	-1.8	6.9
C ₂₀ -H ₂₁	1.089	0.930	C ₂ -C ₃ -C ₂₂	128.4	126.6	C ₃ -C ₂₀ -C ₂₂ -H ₂₃	0.4	-0.9
C ₂₀ -C ₂₂	1.351	1.339	C ₂₀ -C ₂₂ -H ₂₃	121.1	119.0	C ₃ -C ₂₀ -C ₂₂ -C ₂₄	179.1	179.0
C ₂₂ -H ₂₃	1.084	0.929	C ₂₀ -C ₂₂ -C ₂₄	120.0	121.9	C ₂₀ -C ₂₂ -C ₂₄ -O ₂₅	-4.5	-7.6
C ₂₂ -C ₂₄	1.477	1.476	C ₂₂ -C ₂₄ -O ₂₅	121.6	121.6	C ₂₀ -C ₂₂ -C ₂₄ -C ₂₆	176.2	171.4
C ₂₄ -O ₂₅	1.231	1.226	C ₂₂ -C ₂₄ -C ₂₆	119.1	118.6	C ₂₂ -C ₂₄ -C ₂₆ -C ₂₇	-13.6	-3.0
C ₂₄ -C ₂₆	1.504	1.503	C ₂₄ -C ₂₆ -C ₂₇	123.9	122.9	C ₂₄ -C ₂₆ -C ₂₇ -C ₂₈	-179.0	-177.5
C ₂₆ -C ₂₇	1.402	1.395	C ₂₆ -C ₂₇ -C ₂₈	120.9	121.1	C ₂₆ -C ₂₇ -C ₂₈ -C ₂₉	-0.3	0.4
C ₂₇ -C ₂₈	1.394	1.385	C ₂₇ -C ₂₈ -C ₂₉	119.0	119.8	C ₂₇ -C ₂₈ -C ₂₉ -C ₃₀	0.5	-2.0
C ₂₈ -C ₂₉	1.392	1.379	C ₂₈ -C ₂₉ -C ₃₀	121.2	121.7	C ₂₈ -C ₂₉ -C ₃₀ -C ₃₁	-0.09	2.0
C ₂₉ -C ₃₀	1.395	1.388	C ₂₉ -C ₃₀ -C ₃₁	118.9	118.6	C ₂₄ -C ₂₆ -C ₂₇ -H ₃₂	-0.49	2.55
C ₃₀ -C ₃₁	1.390	1.382	C ₂₆ -C ₂₇ -H ₃₂	120.7	119.3	C ₂₆ -C ₂₇ -C ₂₈ -H ₃₃	179.4	-179.5
C ₂₇ -H ₃₂	1.084	0.931	C ₂₇ -C ₂₈ -H ₃₃	120.7	120.5	C ₂₈ -C ₂₉ -C ₃₀ -H ₃₄	179.7	-178.0
C ₂₈ -H ₃₃	1.083	0.929	C ₂₉ -C ₃₀ -H ₃₄	120.1	120.6	C ₂₉ -C ₃₀ -C ₃₁ -H ₃₅	179.3	179.8
C ₃₀ -H ₃₄	1.083	0.931	C ₃₀ -C ₃₁ -H ₃₅	120.8	119.3	C ₂₇ -C ₂₈ -C ₂₉ -Br ₃₆	-179.5	176.8
C ₃₁ -H ₃₅	1.084	0.929	C ₂₈ -C ₂₉ -Br ₃₆	119.3	118.8			
C ₂₉ -Br ₃₆	1.910	1.908						

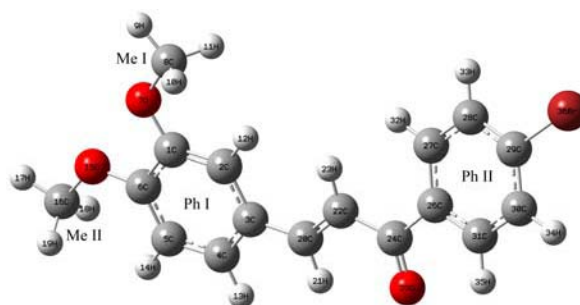


Figure 4. Molecular structure and atomic numbering of DMBC.

4.3 NBO analysis

NBO analysis provides an efficient method for studying the interactions in both filled and virtual orbital spaces that could enhance the analysis of intra and inter molecular interactions. The NBO calculation have been performed using NBO 3.1 program as implemented in the Gaussian '09 package at the DFT/B3LYP 6-31 G(d,p) level, and it gives information about intra molecular hydrogen bonding, delocalisation of electron density and intra molecular charge transfer(ICT) within the molecule. The second order perturbation theory analysis of Fock matrix in NBO basis shows strong intra molecular hyper conjugative interactions of π electrons, which are presented in table 2. Larger the E (2) values, the more intensive the interaction between electron donors and electron acceptors and greater the extent of conjugation of the whole system [34, 35]. The hyperconjugative interaction energy deduced from the second order perturbation approach is

$$E(2) = -n_{\sigma} \frac{\langle \sigma | F | \sigma^* \rangle^2}{\epsilon_{\sigma^*} - \epsilon_{\sigma}} = -n_{\sigma} \frac{F_{ij}^2}{\Delta E} \quad (3)$$

where $\langle \sigma | F | \sigma^* \rangle^2$ or F_{ij}^2 is the Fock matrix element of the i and j NBO orbitals, ϵ_{σ} and ϵ_{σ^*} are the energies of σ and σ^* NBOs and n_{σ} is the population of the donor σ orbital.

The strong intra molecular hyper conjugative interactions of the σ and π electrons of the C-C bond with the C-C anti bond of both the phenyl rings lead to stabilization of the system. The transfer of charge taking place within the molecule is more in $\pi \rightarrow \pi^*$ transition. The intra molecular C-H \cdots O

hydrogen bond exposed in the NBO analysis is formed by the orbital overlap between LP (O) and σ^* (C-H). The stabilization energy $E(2)$ associated with $n_2(O_{25}) \rightarrow \sigma^*(C_{20}-H_{21})$ interaction is 0.52 kJ mol^{-1} , which indicates the possibility of weak intra molecular hydrogen bonding. Due to rehybridization, the C-H bond distance is strengthened, shortened and blue shifted in the stretching wave number. The analysis reveals that charge transfer takes place from lone pairs $n(O_7)$ and $n(O_{15})$ of the methoxy oxygen atom to the π orbitals of phenyl ring Ph1 with interaction energy 30.60 and $31.54 \text{ kJ mol}^{-1}$, respectively.

Table 2. Second order perturbation theory analysis of Fock matrix in NBO basis of DMBC at the B3LYP/6-31 G(d,p) level of theory.

Donor (i)	ED(i) (e)	Acceptor(j)	ED(j) (e)	$E(2)^a$ (kJ mol^{-1})	$E(j)-E(i)^b$ (arbitr.units)	$F(i,j)^c$ (arbitr.units)
πC_1-C_2	1.7241	$\pi^*C_3-C_4$	0.3756	17.59	0.31	0.067
		$\pi^*C_5-C_6$	0.3754	17.90	0.30	0.067
πC_3-C_4	1.6603	$\pi^*C_1-C_2$	0.3467	18.72	0.28	0.065
		$\pi^*C_5-C_6$	0.3754	18.52	0.28	0.065
		$\pi^*C_{20}-C_{22}$	0.1243	17.41	0.30	0.068
C_5-C_6	1.6882	$\pi^*C_1-C_2$	0.3467	17.46	0.30	0.065
		$\pi^*C_3-C_4$	0.3756	19.59	0.31	0.070
$\pi C_{28}-C_{29}$	1.6745	$\pi^*C_{26}-C_{27}$	0.3616	19.12	0.31	0.069
$\pi C_{30}-C_{31}$	1.6530	$\pi^*C_{26}-C_{27}$	0.3616	19.34	0.29	0.067
		$\pi^*C_{28}-C_{29}$	0.3795	22.93	0.27	0.071
LP(1) O_7	1.9644	$\sigma^*C_1-C_2$	0.0234	7.26	1.13	0.081
LP(2) O_7	1.8421	$\pi^*C_1-C_2$	0.0234	30.60	0.34	0.096
LP(2) O_{15}	1.8294	$\pi^*C_5-C_6$	0.3754	31.54	0.34	0.098
LP(2) O_{25}	1.8885	$\sigma^*C_{20}-H_{21}$	0.0189	0.52	0.74	0.018
		$\sigma^*C_{24}-C_{26}$	0.0639	19.29	0.70	0.105
$\pi^*C_5-C_6$	0.3754	$\pi^*C_3-C_4$	0.3756	256.67	0.01	0.081
$\pi^*C_{24}-O_{25}$	0.2141	$\pi^*C_{20}-C_{22}$	0.1243	43.76	0.03	0.072
$\pi^*C_{28}-C_{29}$	0.3795	$\sigma^*C_{26}-C_{27}$	0.0234	196.48	0.02	0.085
		$\sigma^*C_{30}-C_{31}$	0.2856	139.99	0.02	0.081

^a $E(2)$ is the energy of hyperconjugative interactions.

^b Energy difference between donor and acceptor i and j NBO orbitals.

^c $F(i, j)$ is the Fock matrix element between i and j NBO orbitals.

4.4 Thermal studies

The result of the TGA/DTA analysis is shown in figure 5. DTA curve shows that the material undergoes an irreversible endothermic transition where melting begins. The peak of the endothermic at 124.71 °C where melting terminates, corresponds to its melting point and it is clear that there is no phase transition before melting. The sharpness of the peak shows good crystallinity and purity of the sample. TGA curve of the sample indicates that the sample is stable up to 265.0 °C. The endothermic peak of DTA at 315.49 °C corresponds to the first phase of weight loss in the TG curve, indicating decomposition of the sample. This endothermic peak is followed by an exothermic peak at 380.0 °C indicating evaporation of the decomposed compound.

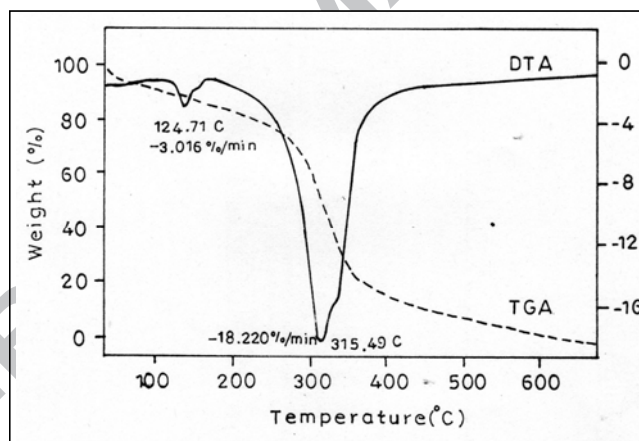


Figure 5 The TGA/DTA curves of the DMBC crystal.

4.5 Absorption spectra

The electronic spectra of DMBC were calculated using the Gaussian '09 program, [27] at the B3LYP/6-31 G (d,p) level. The observed and simulated UV-Vis spectra are shown in figure 6. The electronic transitions and the corresponding excitation energies are listed in table 3. The computed results (table 3) show that the HOMO (highest occupied molecular orbital) to LUMO (lowest unoccupied

molecular orbital) transition corresponds to the λ_{\max} absorption band in the UV-vis spectrum. From the calculations in the gas phase it is seen that the frontier level HOMO has the molecular orbital number 88 with 'A' symmetry and the LUMO has the molecular orbital number 89 with the same 'A' symmetry. The strong band observed experimentally at 355 nm was calculated at 367 nm in the gas phase corresponding to HOMO to LUMO excitation, with the highest oscillator strength. The analyses of the molecular orbital coefficients based on the optimized geometry indicate that the band is originated by an $n \rightarrow \pi^*$ transition. The other transitions are calculated at 378 nm and 312 nm, with lower oscillator strengths.

Table 3: Experimental and Calculated absorption wavelengths, energies and oscillator strengths of DMBC using the TD-DFT method at the B3LYP/6-31G(d,p) level.

Excitation	CI expansion Coefficient	Wavelength (nm) Calc. Gas phase	Oscillator Strength (f)	Wavelength (nm) Expt.
Excited state 1	Singlet-A	378.0	0.002	
85→89	0.46127			
86→89	0.43686			
87→89	-0.20944			
88→89	-0.11385			
Excited state 2	Singlet-A			
86→89	0.11061	367.0	0.619	355
87→89	-0.13061			
88→89	0.62973			
Excited State 3	Singlet-A			
86→89	0.30184	312.0	0.200	
87→89	0.59767	367.0	0.619	
88→92	-0.11319			

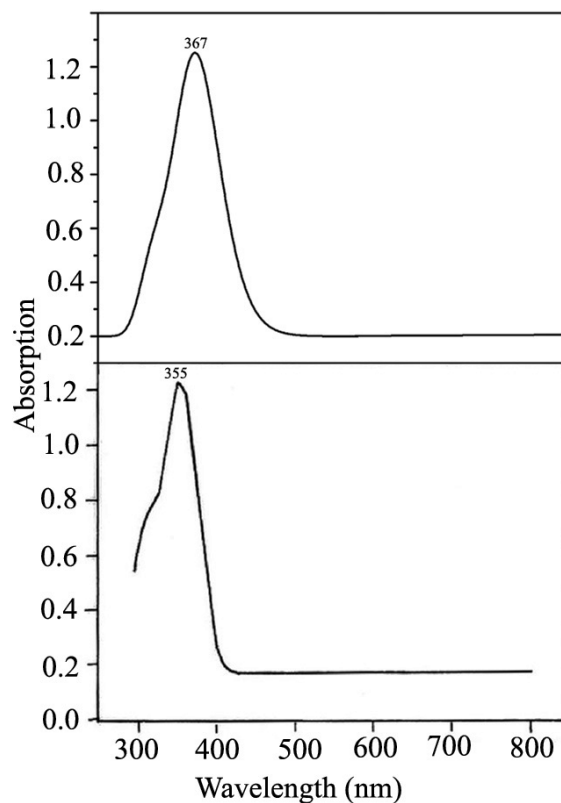


Figure 6. Simulated electronic absorption spectra of DMBC at the B3LYP/6-31G (d, p) level gas phase (top) UV-VIS spectra of DMBC molecule recorded in gas phase (bottom).

The HOMO and LUMO plot of DMBC, as implemented within the Gauss View Version 5.1 program, is shown in figure 7. The HOMO represents the ability to donate an electron, whereas, LUMO as an electron acceptor, represents the ability to obtain an electron. Energy difference between the HOMO and LUMO orbital is called energy gap, which is an important stability reflector for structures. A low HOMO–LUMO gap implies lower stability of the molecule in the sense of its higher charge transfer in compounds. The conjugated molecules are characterized by a small HOMO-LUMO separation, which is the result of a significant degree of ICT from the electron-donor groups to the efficient electron-acceptor groups through the π conjugated path. The HOMO and LUMO energies are -546.18 kJ/mol and -198.96 kJ/mol at the DFT level. The energy gap 347.22 kJ/mol reflects the lowering of energy gap and hence the

enhanced biological activity of the molecule. Moreover the lowering of the HOMO and LUMO energy gap explains the eventual charge transfer interactions taking place within the molecule.

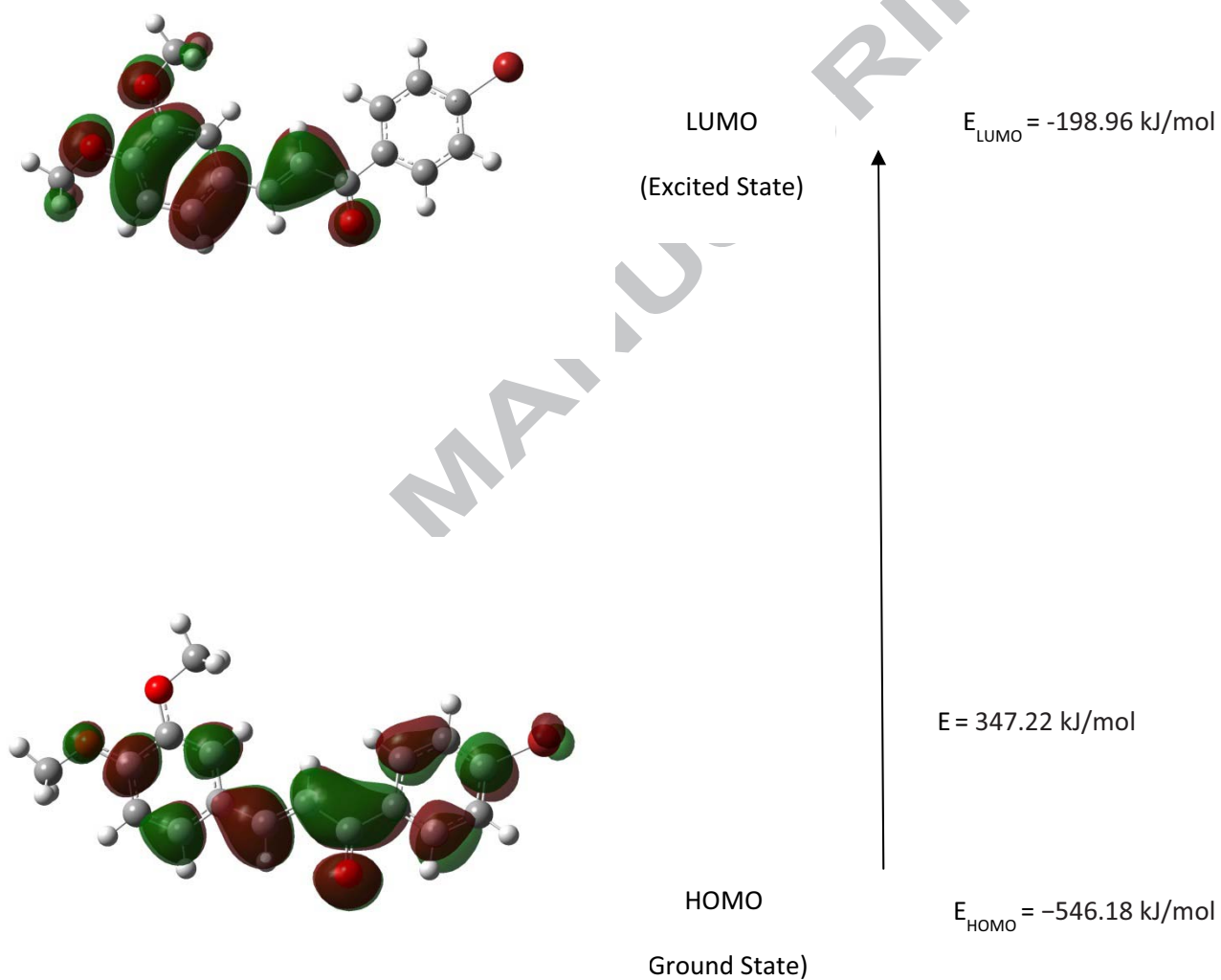


Figure 7. HOMO LUMO plot of DMBC by B3LYP/6-31G(d,p) level of theory.

4.6 Vibrational spectral analysis

The detailed vibrational spectral analysis of DMBC was performed based on the normal coordinate analysis according to the scaled quantum mechanical (SQM) force field methodology. The potential energy distribution (PED) reveals that many of the internal modes contribute to a particular vibrational mode and involve the simultaneous motion of a large number of atoms. The observed and calculated wavenumbers together with the infrared and Raman intensities and normal modes description (characterized by PED) of DMBC are reported in table 4. A comparison of the observed and simulated IR and FT-Raman spectra of the title compound are presented in figures 8 and 9, which help to understand the observed spectral features. The calculated spectra were found to be close to the experimental values with reasonable degree of accuracy. H-atoms involved in intermolecular H-bonds give rise to deviations of the simulated spectra from the experimental spectra, which is attributed to the fact that the theoretical spectrum was obtained in gas phase without considering the inter-molecular H-bonding effects.

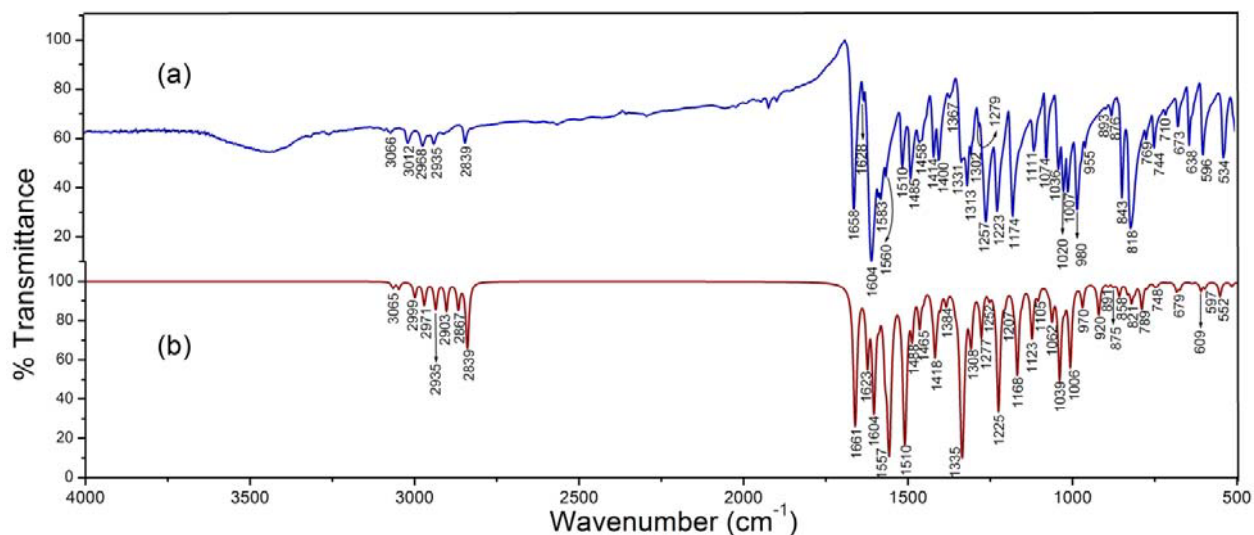


Figure 8. (a) Experimental FT-IR spectra in the range 4000–400 cm^{-1} and (b) Simulated IR spectra of DMBC by B3LYP/6-31G(d,p) level of theory.

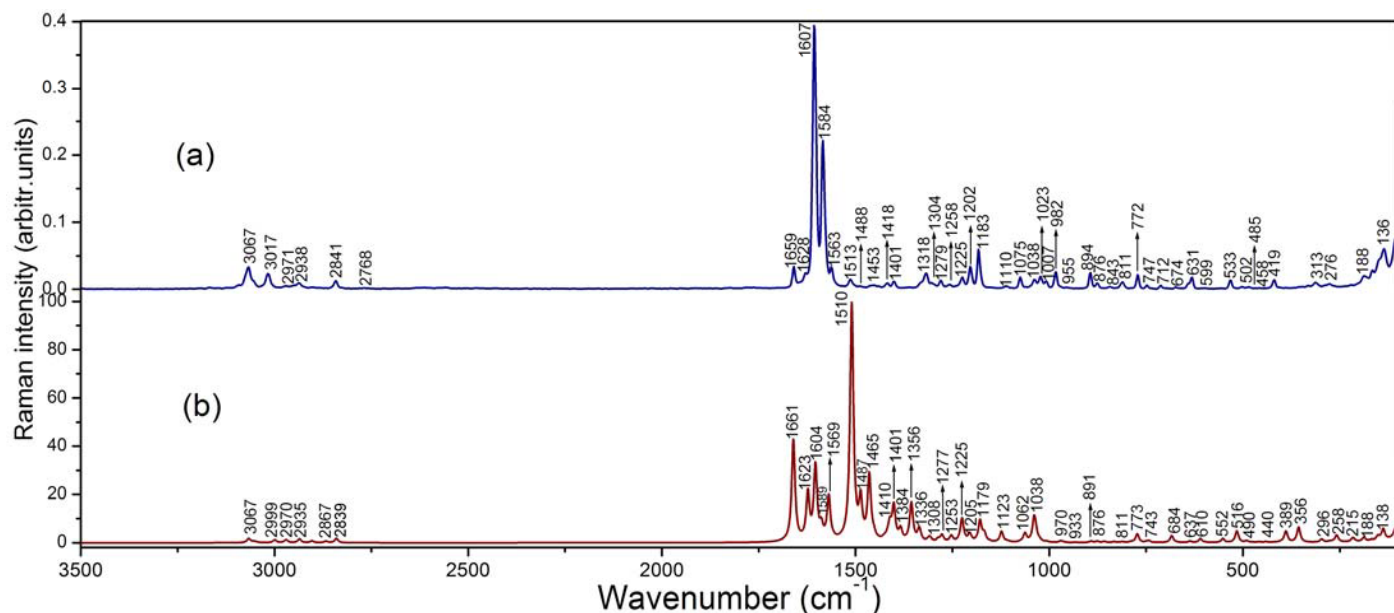


Figure 9. (a) Experimental FT-Raman spectra in the range 3500–50 cm⁻¹ (b) Simulated Raman spectra of DMBC at the B3LYP/6-31G(d,p) level of theory.

4.6.1 Methoxy group vibrations. The methoxy C-H symmetric stretching mode usually appear in the region 2825-2870 cm⁻¹ where as asymmetric mode lie in the range 2925-2985 cm⁻¹ [36, 37]. The weak infrared band at 2968 cm⁻¹ and the corresponding weak Raman band at 2971 cm⁻¹ are assigned to CH₃ asymmetric stretching (CH₃ ops) vibration. The weak infrared band at 2935 cm⁻¹ and the corresponding weak Raman band at 2938 cm⁻¹ are assigned to CH₃ in-plane stretching modes. The symmetric CH₃ stretching band is observed at 2839 cm⁻¹ as a weak IR band and at 2841 cm⁻¹ as a weak Raman band, which is calculated at 2839 cm⁻¹. Though the calculated asymmetric and symmetric stretching wavenumbers arising from different O-CH₃ groups show slight differences in wavenumber, they could not be separated out in the spectra. The asymmetric and symmetric bending vibrations of methyl group are expected in the region 1465-1440 cm⁻¹ and 1390-1370 cm⁻¹ respectively [36,37]. The methyl asymmetric deformation appears as a medium band in IR at 1458 cm⁻¹ and a weak band in Raman at 1453 cm⁻¹. The methyl frequencies are to some extent sensitive to the electro negativity of the attached atom

and the symmetric deformation is particularly sensitive and it appears at 1400 cm^{-1} in IR and 1401 cm^{-1} in Raman. The rocking vibrations of the CH_3 group generally appear as mixed vibrations in the range $1070\text{--}1010\text{ cm}^{-1}$. The strong band in IR at 1174 cm^{-1} and the medium band in Raman at 1183 cm^{-1} are assigned to CH_3 rocking mode.

Table 4. Detailed assignment of fundamental vibrations of DMBC by NCA based on SQM force field calculations.

Calculated wavenumbers (cm^{-1})		Observed wavenumbers (cm^{-1})		IR Intensity ^a	Raman Intensity ^b	Characterization of normal modes with PED ^c (%)
Unscaled	Scaled	FTIR	Raman			
3232	3067	3066vw	3067w	3.51	11	$\nu_{20b}\text{CH}_{\text{ph1}}$ (99)
3228	3064	-	-	3.56	2.79	$\nu_{20a}\text{CH}_{\text{ph1}}$ (99)
3228	3055	-	-	0.23	3.66	$\nu_{20b}\text{CH}_{\text{ph2}}$ (98)
3225	3047	3012 w	-	9.51	2.49	$\nu_{20a}\text{CH}_{\text{ph2}}$ (99)
3215	3002	-	3017 w	4.45	2.26	$\nu_2\text{CH}_{\text{ph2}}$ (98)
3213	2998	-	-	17.46	7.56	$\nu_{7a}\text{CH}_{\text{ph2}}$ (57), νCH (41)
3200	2971	-	-	27.07	6.89	$\nu_{7b}\text{CH}_{\text{ph2}}$ (50) , νCH (48),
3195	2967	-	-	6.77	3.44	$\nu_{7b}\text{CH}_{\text{ph1}}$ (98)
3168	2939	-	-	8.63	1.23	νCH (98)
3156	2935	2968 w	2971 vw	32.02	11	CH3_{ops2} (68), CH3_{ips2} (22)
3153	2903	-	-	1.06	2.15	CH3_{ops1} (67), CH3_{ips1} (23), CH3_{ss1} (10)
3084	2903	2935 w	2938 vw	39.52	3.84	CH3_{ips2} (74) CH3_{ops2} (25)
3076	2867	-	-	37.29	5.12	CH3_{ips1} (74), CH3_{ops1} (25)
3020	2841	-	-	20.48	7.3	CH3_{ss2} (89)
3014	2839	2839 w	2841vw	88.91	6.93	CH3_{ss1} (89)
1736	1661	1658 vs	1659 w	340.69	339	νCO (59), νCC (14), δCC (10)
1662	1623	1628 vw	1628 vw	126.04	154	$\nu_{8b}\text{CC}_{\text{ph1}}$ (35), νCC (26)
1642	1604	1604 vs	1607 vs	269.67	248	$\nu_{8a}\text{CC}_{\text{ph2}}$ (32), $\nu\text{CC}_{\text{ph2}}$ (22), νCC (11)
1637	1588	1583 w	1584 s	25.03	42.5	$\nu_{8b}\text{CC}_{\text{ph2}}$ (46), $\delta\text{CH}_{\text{ph2}}$ (13)
1622	1569	-	1563 w	109.90	144	$\nu_{8a}\text{CC}_{\text{ph1}}$ (60)
1614	1557	1560 w	-	550.75	2.73	$\nu_{19a}\text{CC}_{\text{ph2}}$ (69), $\delta\text{CH}_{\text{ph2}}$ (10)
1562	1513	1510 m	1510 w	23.75	69.5	$\nu_{19b}\text{CC}_{\text{ph1}}$ (34), $\delta\text{CH}_{\text{ph1}}$ (31), νCO (17)
1525	1510	-	-	430.66	742	$\delta\text{CH}_{\text{ph2}}$ (57), $\nu\text{CC}_{\text{ph2}}$ (39)
1518	1488	-	1488 w	41.81	14.1	CH3_{as1} (61), $\text{CH3}_{\text{asyd1}}$ (21)
1516	1487	1485 s	-	25.11	112	CH3_{as2} (59), $\text{CH3}_{\text{asyd2}}$ (24)
1505	1465	-	-	56.76	214	$\text{CH3}_{\text{asyd2}}$ (48), CH3_{as2} (20), $\text{CH3}_{\text{asyd1}}$ (18)
1504	1453	1458 m	1453 w	13.31	16	$\text{CH3}_{\text{asyd1}}$ (50), $\text{CH3}_{\text{asyd2}}$ (18), CH3_{as1} (18)
1501	1426	-	-	15.39	6.54	CH3_{syd1} (54), $\nu\text{CC}_{\text{ph1}}$ (21)
1487	1418	1414 m	1418 w	107.24	10.5	CH3_{syd1} (54)
1465	1411	-	1510 w	19.10	51.9	$\nu\text{CC}_{\text{ph1}}$ (37), CH3_{syd1} (28), $\delta\text{CH}_{\text{ph1}}$ (15)

1435	1401	1400 m	1401 w	19.23	115	$\nu_{19b}CC_{ph2}(47), \delta CH_{ph2}(39)$
1400	1384	-	-	22.06	37.8	$\nu_{19a}CC_{ph1}(58), \delta CCH(14)$
1363	1356	1367 w	-	14.06	129	$\delta CCH(28), \nu CC_{ph1}(19), \nu CC_{ph2}(18), \nu CC(14)$
1349	1336	1331 w	-	590.02	43	$\nu_{14}CC_{ph1}(28), \delta CCH(21), \delta CH_{ph1}(15)$
1342	1313	1313 s	1318 w	15.73	3.19	$\nu_{14}CC_{ph2}(89)$
1323	1308	1302 vw	1304 w	76.98	14.4	$\delta_3 CH_{ph2}(61)$
1316	1287	-	-	4.26	8.24	$\nu CC_{ph1}(28), \nu CO_{ph1}(26), \delta CH_{ph1}(13)$
1306	1277	1279 vw	1279 w	75.76	22.2	$\delta CH_{ph1}(54), \nu CC_{ph1}(11), \delta CCH(10)$
1276	1253	1257 vs	-	12.82	19.3	$\nu CO_{ph1}(30), R_{trid}(13),$
1233	1225	1223 vs	1225 w	275.63	78.6	$\nu_{9a}CC_{ph2}(42), \delta CCH(27)$
1226	1205	-	1202 w	17.47	25.7	$\delta OM1(27), \nu CC_{ph1}(21)$
1214	1179	1174 vs	1183 m	14.10	70.1	$\delta OM2(44), \delta OM1(15), CH_3_{ipr}(13)$
1205	1168	-	-	158.45	26.5	$CH_3_{ipr1}(71), CH_3_{opr1}(23)$
1195	1154	-	-	11.95	2.19	$CH_3_{ipr2}(72), CH_3_{opr2}(21)$
1179	1123	-	-	83.46	34.9	$\delta CH_{ph2}(62), \nu CC_{ph1}(16)$
1177	1110	1111 m	1110 vw	0.977	2.29	$\nu_{18b}CC_{ph1}(19), \delta OM1(12), \delta CH_{ph1}(11)$
1174	1104	-	-	16.89	2.14	$\delta CH_{ph1}(50), \nu CC_{ph1}(25)$
1133	1074	1074 s	1075 w	4.61	1.81	$\delta CH_{ph2}(59), \nu CC_{ph2}(33)$
1090	1063	-	-	48.92	28.3	$\nu CC_{ph2}(62), \delta CH_{ph2}(18), \nu CBr(15)$
1081	1039	1036 m	1038 w	167.37	70.1	$\nu OC_1(41), \nu OC_2(33), \nu CC_{ph1}(14)$
1061	1035	-	-	9.42	29.9	$\nu OC_2(40), R_{trid1}(25), \nu OC_1(20)$
1055	1024	1020 s	1023 w	17.38	5.11	$\nu CC(35), \nu CC_{ph2}(28)$
1034	1007	1007s	-	142.40	2.97	$gCHC(56), tCCH(29)$
1022	970	980 s	982 w	32.11	5.85	$R_{trid2}(25), \nu CC_{ph2}(12)$
1007	962	955 w	-	0.15	1.09	$R_{asyto2}(45), R_{puck2}(36), R_{wag2}(18)$
994	933	-	-	0.70	0.867	$\nu CC_{ph1}(38), \nu OC_1(12), \delta CCC(11), \nu CO_{ph1}(10)$
972	920	-	-	46.25	0368	$R_{puck2}(46), R_{asyto2}(30), R_{wag2}(24)$
927	891	893 w	894 m	3.50	4.97	$R_{wag1}(86), R_{puck1}(7)$
885	876	876 w	876 w	4.73	4.33	$R_{wag2}(35), g_{10b}CHC(25), gOCC(11)$
872	858	843 m	843 vw	18.07	3.82	$\delta CCC(25), \delta CCO(16), \nu CC_{ph2}(15)$
860	833	-	-	12.23	2.99	$R_{wag2}(36), R_{wag1}(28), gCHC(15)$
855	821	818 vs	-	25.44	0.707	$R_{wag1}(64), R_{wag2}(13)$
842	811	-	811 w	10.48	0.261	$R_{wag2}(74)$
817	789	-	-	37.63	0.263	$R_{wag1}(69)$
789	773	769 w	772 w	5.26	27.9	$10a \nu CC_{ph1}(28), \nu CO_{ph1}(22), R_{asyd}(11)$
761	749	-	747 w	4.98	2.41	$R_{puck2}(49), R_{asyto2}(47)$
749	743	744 m	-	3.94	5.9	$R_{puck2}(23), R_{asyto2}(22), R_{asyd}(11)$
716	712	710 w	712 w	0.69	0.769	$R_{puck2}(42), R_{asyto2}(40)$
698	684	-	-	11.80	21.9	$R_{puck2}(44), R_{asyto2}(41)$
690	674	673 m	-	9.26	1.19	$4 R_{puck2}(49), R_{asyto2}(46)$
643	637	638m	631vw	1.75	4.66	$R_{asydO}(84)$
627	610	603 vw	-	11.76	12.3	$\nu CO_{ph1}(35), \delta COC(25), \delta CCC(11)$
614	597	596 m	-	7.76	1.09	$6a R_{wag1}(32), R_{puck2}(17), R_{asyto2}(15), R_{asyt1}(14)$

564	552	534 m	533 vw	19.90	12.2	vCBr(16), 6b vCC _{ph2} (15), R _{wag2} (12), R _{asyt 2} (12)
530	516	-	-	5.82	37.6	R _{asydo1} (20), R _{asyd1} (20), δ COC(17), vCC _{ph1} (15)
493	490	-	-	4.87	5.61	R _{wag2} (23), R _{asyt 2} (22), R _{asyd1} (17), δ CCC(37)
482	476	-	-	10.33	1.06	R _{wag2} (28), R _{asyt 2} (27)
473	459	-	-	4.47	2.25	δ CCC(37)
467	440	-	-	0.01	2.53	R _{wag1} (48), R _{asyt2} (29), R _{asyt1} (12)
422	417	-	419 w	0.20	0.986	R _{asyt2} (82), R _{wag2} (15)
409	401	-	-	2.30	1.8	R _{wag1} (40), R _{puck1} (13), R _{asyt1} (12), R _{asyt2} (10)
385	389	-	-	5.37	36.4	δ COC(38), δ COC(23), vCO _{ph1} (11), δ CCC(10)
367	356	-	-	25.49	49.9	vCC _{ph2} (18), δ COC(14), vCC _{ph1} (11)
297	297	-	316 w	0.23	9.44	δ CBr(22), R _{asyt2} (10), R _{puck2} (13), δ CC(12)
289	279	-	-	0.13	1.51	tCOCH(48), R _{wag1} (16), R _{asyt1} (10)
272	272	-	276 w	0.07	2.04	vCBr(23), R _{asyd} (13)
265	265	-	-	2.04	0.682	R _{puck2} (40), R _{asyt2} (36), R _{wag2} (17)
258	258	-	-	0.84	22	tCOCH(48), R _{asyt1} (36)
224	217	-	-	0.62	6.8	tCOCH(24), R _{asyt1} (21), R _{wag1} (13)
219	214	-	-	0.41	7.15	δ CBr(23), δ CCC(9), δ CO(16)
194	188	-	188 vw	5.82	12.4	δ CO(45), δ CBr(12)
174	168	-	-	0.04	3.55	R _{asyt2} (25), R _{puck1} (21), R _{asyt1} (10)
155	151	-	-	1.02	13.4	δ CCC(15), vCC _{ph2} (14), vCC _{ph1} (12), R _{asyd2} (11)
141	138	-	136 m	0.42	36.2	tHCCO(14), tCCCH(11)
115	107	-	-	0.28	16.2	tCCOC(34), tCOCH(12)
100	96	-	-	0.33	82.1	tCCOC(15), tHCCCH(10)
91	89	-	-	12.41	5.06	tCCOC(53), tCOCH(19)
77	77	-	-	0.37	21.1	R _{wag2} (22), tOCCC(15), R _{asyt2} (13)
54	52	-	-	0.29	78.7	R _{wag1} (15), tCCOC(15), R _{asyt1} (13)
33	33	-	-	0.01	456	δ CCC(43), tOCCC(48)
23	25	-	-	0.01	981	tOCCC(48), δ CCC(18)
13	12	-	-	0.21	2830	tCCCH(40), tHCCO(32)

vs: very strong; ms: medium strong; s: strong; w: weak; vw: very weak

v: stretching; ph1: phenyl ring1; ph2: phenyl ring2; t: torsion; g: gauche; wag: wagging; ss: symmetric stretching; as: asymmetric stretching; sd: symmetric deformation; ips: in plane stretching; ops: out of plane stretching; ipb: in plane bending; opb: out of plane bending; sb: symmetric bending; rck: rocking; ipr: in plane rocking; opr: out of plane rocking; ; R: ring; trid: trigonal deformation; asyd: asymmetric deformation; asydo: out of plane asymmetric deformation; puck: puckering; asyt: asymmetric torsion; asyto: out of plane asymmetric torsion; sc: scissoring;

^a Relative absorption intensities normalized with highest peak absorption equal to 1.

^b Relative Raman intensities calculated by Eq. (1) and normalized to 100.

^c Only potential energy distribution greater than 10%.

4.6.2 Phenyl ring vibrations. Aromatic structures show characteristic C-H stretching vibrations occurring in the region 3100-3000cm⁻¹ [36-39]. Wilsons numbering convention is used in the vibrational assignment

of the phenyl rings [40]. The C–H stretching vibrations in benzene derivatives arise from two non degenerate modes a_{1g} (3072 cm^{-1}), b_{1u} (3060 cm^{-1}) and two degenerate modes e_{2g} (3047 cm^{-1}), e_{1u} (3099 cm^{-1}), i.e. vibrations 2, 13, 7 and 20, respectively. The DMBC molecule comprises of one tri-substituted phenyl ring (Ph1) and para-disubstituted phenyl ring (Ph2). In para-disubstituted phenyl rings, 2, 7a, 20a and 20b are active where as in tri-substituted benzenes, of the four allowed C-H stretching modes 2, 20b, 20a and 7b, except 20a, all allowed ring modes are found to be active. Most of the C-H stretching vibrations are found to be weak which is due to the charge transfer from the hydrogen atom to the carbon atom. The mode 20b is active in IR with a weak band at 3066 cm^{-1} and its counterpart weak Raman band at 3067 cm^{-1} . The normal mode 2 appears as a weak band in Raman at 3017 cm^{-1} and as a weak band in IR at 3012 cm^{-1} . Normal vibrations 3, 9a, 15, 18a and 18b are the C-H in plane bending vibrations of the substituted phenyl rings and can be expected in the region $1300\text{-}1000\text{ cm}^{-1}$. The in plane deformation mode 3 is observed in IR at 1302 cm^{-1} and 1304 cm^{-1} in Raman. The strong IR and weak Raman bands at 1223 cm^{-1} and 1225 cm^{-1} respectively, correspond to the vibrational mode 9a. The weak band at 1111 cm^{-1} in IR is assigned to the 18b mode of ring Ph1. The absorption bands arising from C–H out-of-plane bending vibrations are usually observed in the region $1000\text{-}675\text{ cm}^{-1}$. The out-of-plane vibrations in benzene arise from b_{2g} (995 cm^{-1}), e_{2u} (975 cm^{-1}), e_{1g} (849 cm^{-1}) and a_{2u} (671 cm^{-1}) modes of benzene. The 10a mode appears in IR as a weak band at 769 cm^{-1} and as a weak band at 772 cm^{-1} in Raman, corresponding to Ph1. The phenyl ring modes 4, 6a, and 6b can be observed in IR spectrum at 673 cm^{-1} , 596 cm^{-1} and 534 cm^{-1} respectively.

The ring stretching vibrations are prominent in the vibrational spectra of benzene and its derivatives, as the double bond is in conjugation with the ring. The phenyl ring gives rise to six ring stretching modes (8a, 8b, 19a, 19b, 14 and 1), which are more sensitive to substituents [40]. With heavy substituents, the bands tend to shift to somewhat lower wavenumbers and the greater the number of substituents on the ring, the broader the absorption regions [40]. The mode with the highest magnitude

corresponds to the doubly degenerate mode e_{2g} (mode 8) of benzene (1599 cm^{-1}) which splits into two components (8a, 8b) for substituted benzenes. DFT computation gives vibrational modes at 1569 cm^{-1} and 1623 cm^{-1} corresponding to 8a mode and 8b mode of Ph1 respectively and at 1604 cm^{-1} and 1588 cm^{-1} respectively corresponding to ring Ph2. The ring mode 8b of Ph1 manifests as a medium shoulder band around 1628 cm^{-1} in IR and as an intense Raman band near 1628 cm^{-1} . Its relatively strong companion 8a appears at 1563 cm^{-1} in IR. The phenyl ring mode 8b is observed as a weak band in the IR spectra at 1583 cm^{-1} and an intense band near 1584 cm^{-1} in Raman is assigned to the para-disubstituted phenyl ring (Ph2). Similarly, the ranges for the degenerate modes e_{1u} (19a and 19b) are $1520\text{ cm}^{-1} - 1460\text{ cm}^{-1}$ and $1420\text{ cm}^{-1} - 1370\text{ cm}^{-1}$ respectively [41]. The observed IR band at 1560 cm^{-1} is assigned to 19a mode of ring Ph2, while the corresponding 19b mode appears as a medium band at 1400 cm^{-1} in IR and as a medium band at 1401 cm^{-1} in Raman. The observed weak band in IR at 1331 cm^{-1} is assigned to the mode 14 of Ph2. In Ph1 the ring mode 14 is observed as a medium band in IR at 1313 cm^{-1} and as a weak band in Raman at 1318 cm^{-1} .

4.6.3 Carbonyl and ethylenic bridge vibrations. The spectral signature of the C=O group is its stretching vibration which appears as an intense band between $1760-1730\text{ cm}^{-1}$ [37, 41]. The position of the C=O stretching vibration is very sensitive to various factors such as the physical state, electronic effects by substituents, ring strains, etc. The C=O stretching vibrations give rise to characteristic intense bands in IR and Raman, and the intensity of these bands can increase owing to conjugation or formation of hydrogen bonds[42]. The $C_{24}=O_{25}$ stretching is observed in IR as a strong band at 1658 cm^{-1} and a weak band in Raman at 1659 cm^{-1} , which are confirmed by their PED values. DFT calculations observed at 1661 cm^{-1} gives the wavenumber of this mode. The deviation from the calculated wave number for this mode can be attributed to the under estimation of π -electron delocalisation due to conjugation and hydrogen bonding network inside the crystal. In DMBC the C=C stretching vibrations of ethylenic bridge overlaps with vibrations of $C_{24}=O_{25}$ stretching mode and C-H bending vibrations. The intense band at 1257 cm^{-1} in IR

spectrum have been assigned to C–O stretching mode which is coupled with C-C stretch and ring trigonal deformation.

4.6.4 C-Br Vibrations. Generally, characteristic C-Br stretching vibration is observed in the region 650-485 cm^{-1} . In the title compound DMBC, a medium band is observed at 534 cm^{-1} in IR. This mode is a pure stretching mode, but it is often influenced by neighboring atom or groups [42-43]. The vibrations belonging to the bond between the ring and the bromine atom are important, as mixing of vibrations are possible due to the presence of the heavy atom. The in plane and out of plane vibrations of C-Br vibration is also coupled with other modes, as evident from the PED values.

4.7 Molecular electrostatic potential

The ESP, $V(r)$, at a point r due to a molecular system with nuclear charges $\{Z_A\}$ located at $\{R_A\}$ and electron density $\rho(r)$ is given by

$$V(r) = \sum_{A=1}^N \frac{Z_A}{|r - R_A|} - \int \frac{\rho(r') d^3 r'}{|r - r'|} \quad (4)$$

The graphical representation of the molecular electrostatic potential surface (MEP or ESP), as described by Kollman and Singh [44] is a series of values representing the evaluation of the interaction energy between a positively charged (proton) probe and points on a solvent accessible surface as defined by Connolly [45]. As implemented within the Gauss View version 5.1 program, areas of high electron density, representing a strong attraction between the proton and the points on the molecular surface, have the brightest red colour and areas of the lowest electron density have deep blue to indigo colour indicating the regions of maximum repulsion. The molecular electrostatic potential (ESP) at a point in the space around a molecule gives an indication of the net electrostatic effect produced at that point by the total charge distribution (electron + nuclei) of the molecule and correlates with dipole moments, electronegativity, partial charges and chemical reactivity of the molecule. It provides a visual method to understand the relative polarity of the molecule. An electron density isosurface mapped with electrostatic potential surface depicts the size, shape, charge density and site of chemical reactivity of the molecules.

The different values of the electrostatic potential at the surface are represented by different colours; red represents regions of most negative electrostatic potential, blue represents regions of most positive electrostatic potential and green represents regions of zero potential. The potential increases in the order red < orange < yellow < green < blue. Molecular electrostatic potential mapped on the $\rho(\mathbf{r}) = 0.0004$ a.u. isodensity surface for DMBC calculated at the B3LYP/6-311++G(d,p) level of theory is shown in figure 10(a). This figure provides a visual representation of the chemically active sites and comparative reactivity of atoms.

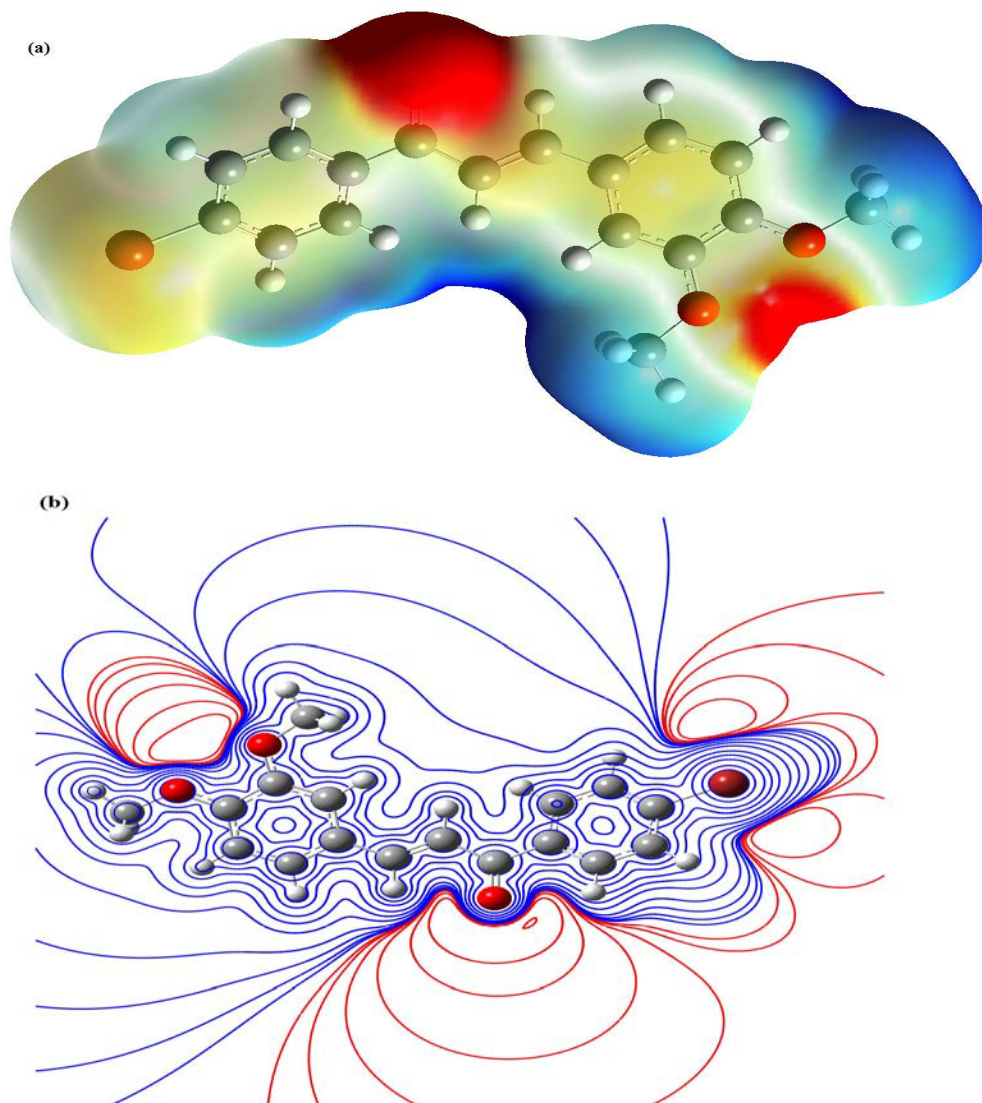


Figure 10(a).Molecular electrostatic potential mapped on the $\rho(\mathbf{r}) = 0.0004$ a.u. isodensity surface for DMBC in the range from $-2.261\text{E-}2$ (red) to $+2.261\text{E-}2$ (blue) (b) Contour diagram for DMBC calculated at the B3LYP/6-311++G(d,p) level of theory.

It may be seen that a region of zero potential envelopes the π -system of the benzene rings, leaving a more electrophilic region in the plane of the hydrogen atoms. The shape of the electrostatic potential surfaces at sites close to the polar carbonyl group in the molecule and the methoxy group is influenced by the stereo structure and the charge density distribution. These sites show regions of the most negative electrostatic potential and high activity of the carbonyl group. In contrast, regions close to the other two polar atoms – bromine, and oxygen of the methoxy groups – show regions of mildly negative potential.

Figure 10 (b) shows the two-dimensional projection of the map into the molecular plane.

5. Conclusions

A chalcone derivative, 1-(4-Bromophenyl)-3-(3, 4-dimethoxy-phenyl) prop-2-en-1-one has been synthesized and small crystals are grown by slow evaporation technique. Density functional theory calculations at the B3LYP/6-31G (d, p) level were used to determine the ground state molecular geometry (bond lengths and bond angles), harmonic vibrational wavenumbers, infrared intensities and Raman activities of this compound. Potential energy distributions (PEDs) and normal modes for the spectral data computed at the B3LYP/6-31G (d, p) level, have also been obtained from force-field calculations. The wavenumbers found after scaling of the force field showed very good agreement with the experimentally determined values. A comparison of the theoretical spectra and experimental FT-IR and FT-Raman spectra of the title molecule has been made and complete vibrational assignments of the observed spectra have been proposed. DMBC is thermally stable up to $265.0\text{ }^{\circ}\text{C}$ and optically transparent in the visible region. The NBO analysis, analysis of electrostatic potential map and the HOMO and LUMO analyses,

reveals the significant degree of charge transfer interactions taking place in the molecule which is responsible for the enhanced chemical as well as biological activity of the molecule.

Acknowledgments

The author, Lynnette Joseph thanks the University Grants Commission (UGC), New Delhi, India, for the financial support, Project No. MRP(S)-899/10-11/KLKE002/UGC-SWRO. The authors are highly grateful to Prof. T. Sundius for the Molvib program.

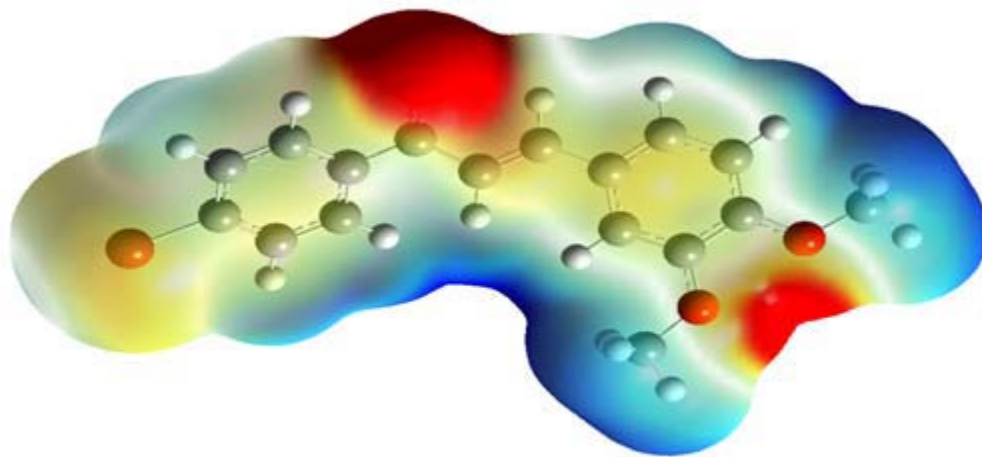
References

- [1] Murakami S, Muramatsu M and Aihara H 1991 *Biochem. Pharmacol.* **42** 1447-51.
- [2] Anto R J, Sukumarana K, Kuttana G, Raob M N A, Subbarajuc V and Kuttana R 1995 *Cancer Lett.* **97** 33-37
- [3] Ducki S, Forrest R, Hadfield J A, Kendall A, Lawrence N J, McGown A T and Rennison D 1998 *Bioorg. Med. Chem. Lett.* **8** 1051-56
- [4] Herencia F, Ferrandiz M L, Ubeda A, Dominguez J N, Charris J E, Lobo G M and Alcaraz M 1998 *J Bioorg. Med. Chem. Lett.* **8** 1169-74
- [5] Liu M, Wilairat P and Go M L 2001 *J. Med. Chem.* **44** 4443-52
- [6] López S N, Castelli M V, Zacchino S A, Dominguez J N, Lobo G, Charris- Charris J, Cortes J C, Ribas J C, Devia C, Rodriguez A M and Enriz R D 2001 *Bioorg. Med.Chem.* **9** 1999-2013
- [7] Wu J H, Wang X H and Yi Y H 2003 *Bioorg. Med. Chem. Lett.* **13** 1813-15
- [8] Mathiesen L, Malterud K E and Sund R B 1995 *Planta Med.* **61** 515-518
- [9] Goto Y, Hayashi A, Kimura Y and Nakayama M J 1991 *Cryst. Growth* **108** 688-698
- [10] Fichou D, Watanabe T, Takeda T, Miyata S, Goto Y and Nakayama M 1988 *Jpn.J.Appl.Phys.* **27** L429-L430
- [11] Kitaoka Y, Sasaki T, Nakai S, Yokotani A, Goto Y and M Nakayama 1990 *Appl.Phys.Lett.* **56** 2074-

- [12] Uchida T, Kozawa K, Sakai T, Aoki M, Yoguchi H I, Atdureyim A and Watanabe Y, 1998 *Mol.Cryst.Liq.Cryst.* **315** 135-140
- [13] Ravindra H J, Chandrashekar K, Harrison W T A and Dharmaprasad S M 2009 *Appl. Phys.* **B 94** 503-511
- [14] Ng S L, Shettigar V, Razak I A, Fun H K, Patil P S and Dharmaprasad S M 2006 *Acta Cryst.* **E62** o1570-72
- [15] Korth H G, de Heer M I and Mulder P 2002 *J. Phys. Chem.* **106** 8779-89
- [16] Chowdhry P K 2003 *J. Phys. Chem.* **A 107** 5692-96
- [17] Chis V 2004 *Chem. Phys.* **300** 1-11
- [18] Asensio A, Kobko N and Dannenberg J J 2003 *J. Phys. Chem.* **A 107** 6441-43
- [19] Rauhut G and Pulay P *J. Phys. Chem.* **99** 1995 3093-3100
- [20] Jensen F 1999 *Introduction to Computational Chemistry* (Wiley, New York)
- [21] Sajan D, Binoy J, Joe I H, Jayakumar V S and Zaleski J 2005 *J. Raman Spectrosc.* **36** 221-236
- [22] Sajan D, Vijayan N, Safakath K, Philip R and Joe I H 2011 *J. Phys. Chem.* **A 115** 8216-26
- [23] Sajan D, Ravindra H J, Misra N and Joe I H 2010 *Vibrational Spectroscopy* **54** 72-80
- [24] Pulay P, Fogarasi G, Pongor G, Boggs J E and Vargha A 1983 *J. Am. Chem. Soc.* **105** 7037-47
- [25] Dhar D N 1981 *The Chemistry of Chalcones and Related Compounds* (Wiley, New York)
- [26] Xiao F Z and Long G Z 2009 *Crystal Growth Des.* **9** 4407-14
- [27] Frisch M J *et.al.* 2010 *Gaussian 09*, C 3 Revision B.01, Gaussian, Inc. (Wallingford, CT).
- [28] G. Fogarasi, X. Zhou, P. W. Taylor, P. Pulay, *J. Am. Chem. Soc.* **114** (1992) 8191-8201.
- [29] Pulay P, Fogarasi G, Pang F, Boggs J E and Vargha A 1979 *J. Am. Chem. Soc.* **101** 2550-60
- [30] Sundius T 1990 *J. Mol. Struct.* **218** 321-26
- [31] Sundius T 2002 *Vib. Spectrosc.* **29** 89-95
- [32] Keresztury G, Holly S, Varga J, Besenyi G, Wang A Y and Durig J R 1993 *Spectrochim. Acta* **A 49** 2007-26

- [33] Keresztury G, Chalmers J M and Griffith P R (Eds.) 2002 *Raman Spectroscopy: Theory in Handbook of Vibrational Spectroscopy*, vol. 1 (John Wiley & Sons Ltd., New York)
- [34] Weinhold F 2001 *Nature* **411** 539-41
- [35] Weinhold F and Landis C 2005 *Valency and Bonding: A Natural Bond Orbital Donor–Acceptor Perspective* (Cambridge University Press, Cambridge)
- [36] Vein D L, Colthup N B, Fateley W G and Grasselli J G 1991 *The Handbook of Infrared and Raman Characteristic Frequencies of Organic Molecules* (Academic Press, New York)
- [37] Silverstein M, Basseler G C, and Morill C 1981 *Spectrometric Identification of Organic Compounds* (Wiley, New York)
- [38] Colthup N B, Daly L H, and Wiberley S E 1990 *Introduction to Infrared and Raman Spectroscopy* (Academic Press, New York)
- [39] Varsanyi G 1974 *Assignments for Vibrational Spectra of 700 Benzene Derivatives* (Adam Hilger, London)
- [40] Bellamy L J 1975 *The Infra-red Spectra of Complex Molecules* (John Wiley and Sons Inc., New York)
- [41] Maroulis G 2003 *J. Mol. Struct. (Theochem)* **633** 177-97
- [42] Michalska D 1993 *Spectrochim. Acta A* **49** 303-14
- [43] Higuchi S 1974 *Spectrochim. Acta A* **30** 463-72
- [44] Singh U C and Kollman P A 1984 *J. Comput. Chem.* **5** 129-45
- [45] Connolly M L 1983 *Science* **221** 709-13

Graphical abstract



Molecular Electrostatic Potential map of the molecule reflects the regions of the most negative electrostatic potential and high activity of the carbonyl group.

Highlights

A chalcone derivative, DMBC has been synthesized and crystals were grown. DFT calculations were used to determine the molecular geometries and vibrational wavenumbers.

Information about the size, shape, charge density distribution and site of chemical reactivity of the molecules has been obtained by mapping the electron density isosurface with electrostatic potential surfaces (ESP)